PNAS RESEARCH ARTICLE | ENVIRONMENTAL SCIENCES

Diffusion-induced instabilities promote cooperation in eco-evolutionary networks

Sourav Roy[a,1], Md Sayeed Anwar[b,1], Timoteo Carletti[c], Matjaž Perc[d,e,f,g,2], and Dibakar Ghosh[h]

Affiliations are included on p. 9.

Edited by Marcus W. Feldman, Stanford University, Stanford, CA; received October 22, 2025; accepted June 12, 2026

Understanding how cooperation persists despite the advantage of selfish behavior remains a central challenge in evolutionary dynamics. Classical models of public goods dilemmas predict dominance of defectors, yet natural and social systems often sustain cooperation. We study an eco-evolutionary public goods game on complex networks where cooperators and defectors diffuse at different rates. When the isolated system is in a defector-dominated coexistence regime, faster dispersal of defectors than cooperators leads to a symmetry-breaking transition that produces localized clusters of cooperators. In heterogeneous networks, nodes with higher connectivity become significantly more likely to exhibit cooperative dominance. A degree-based mean-field reduction supports this result by showing that network connectivity controls an effective coupling strength proportional to node degree, thereby producing a bifurcation that separates defector-dominated and cooperative states. We also address why not all hubs become cooperative by means of a multistability analysis. These results reveal how asymmetric mobility and heterogeneous connectivity jointly promote cooperation in structured populations.

evolutionary biology | complex networks | public goods game | cooperation

Significance

Cooperation underpins the stability of social, ecological, and microbial systems, yet it is continually threatened by defectors that exploit shared resources. We show that asymmetric mobility between cooperators and defectors can fundamentally reshape this conflict in structured populations. When defectors disperse faster than cooperators on complex networks, homogeneous coexistence becomes unstable and heterogeneous spatial patterns emerge. Highly connected nodes are significantly more likely to sustain cooperation, while peripheral nodes remain vulnerable to defection. A mean-field theory explains this behavior by linking node connectivity to an effective coupling strength that governs local dynamics. These results identify differential mobility and network structure as one of the key mechanisms that promote cooperation and provide insights into how movement and spatial heterogeneity shape collective behavior.

The persistence of cooperation in social and biological systems has long been a central point of interest in evolutionary theory. This enduring inquiry traces back to foundational questions about how cooperative traits can survive natural selection when selfish behavior seems evolutionarily advantageous. In well-mixed populations, where each agent interacts with every other one without spatial constraints, traditional game-theoretic models, especially the public goods game, have predicted a grim outcome for cooperation (1, 2). Within these models, defectors, by reaping benefits from shared resources without contributing, consistently outcompete cooperators. This exploitation-driven advantage leads to the eventual extinction of cooperative strategies (3, 4), by resulting in the breakdown of collective action and the depletion of essential environmental resources (5–7). Such theoretical outcomes underscore a central dilemma: If defection is individually advantageous, why is cooperation so pervasive in nature?

Contrary to these theoretical expectations, empirical observations reveal that cooperation is not a rare anomaly but a recurring feature of many biological and social systems, from microbial biofilms to human societies (8–11). These findings suggest that the assumptions of well-mixed populations are often too restrictive to capture real-world dynamics. Natural and social systems typically exhibit spatial structure, ecological feedback, and heterogeneous interactions (12–14). Incorporating such factors into evolutionary models has therefore become essential for understanding how cooperation can emerge and persist.

Several mechanisms have been proposed to support cooperation in structured populations. Spatial structure and limited dispersal allow cooperators to cluster together, thereby protecting themselves from exploitation (15, 16). Reaction–diffusion models have been particularly useful for studying such dynamics, as they describe how local interactions combined with dispersal can generate spatial patterns and cooperative clusters (17). However, these approaches typically assume continuous spatial domains, whereas many biological and social systems operate in discrete environments.

Microbial colonies often grow on patchy substrates, and human interactions frequently occur through discrete social or technological networks (18, 19).

These observations call for modeling frameworks capable of capturing discrete and heterogeneous interaction structures.

Complex networks provide a natural representation of such systems. Prominent examples include scale-free networks with highly connected hubs (20), small-world networks characterized by short path lengths (21), and modular networks with clustered

The authors declare no competing interest.

This article is a PNAS Direct Submission.

[1]S.R. and M.S.A. contributed equally to this work.

[2]To whom correspondence may be addressed. Email: matjaz.perc@gmail.com.

This article contains supporting information online at https://www.pnas.org/lookup/suppl/doi:10.1073/pnas.2530131123/-/DCSupplemental.

Published July 8, 2026.

connectivity (22). In these systems, interactions are governed not by physical distance but by network topology (23). The Laplacian coupling formalism offers a convenient mathematical framework for modeling movement or diffusion across such networks, capturing how the state of each node relaxes toward that of its neighbors. This formulation has been widely used to study diffusion-driven instabilities and pattern formation in networked dynamical systems (24, 25).

Alternative mechanisms for promoting cooperation have also been explored. In particular, models of the iterated Prisoner's Dilemma with partner choice or refusal have shown that allowing individuals to select or avoid interaction partners can stabilize cooperation by enabling cooperators to assort and avoid exploitation (26, 27). In such frameworks, cooperation arises through strategic interaction choices. In contrast, the mechanism considered here does not rely on partner selection. Instead, we focus on how mobility and spatial coupling alone, without active partner choice, can reshape eco-evolutionary dynamics in structured populations.

Despite substantial progress in modeling cooperation on networks, several aspects of eco-evolutionary dynamics remain insufficiently explored. In particular, the combined effects of local group interactions, ecological feedback, and asymmetric mobility between strategies have rarely been integrated into a unified framework. In many real-world systems, cooperators and defectors differ in their mobility or dispersal rates. For instance, defectors may spread more rapidly across environments while cooperators remain localized within productive regions (28–30). Such differences can generate spatial instabilities that reorganize population structure and potentially promote cooperation. From a dynamical perspective, these processes can be interpreted as diffusion-driven instabilities reminiscent of Turing pattern formation (31).

Motivated by these observations, we develop an eco-evolutionary public goods game model on complex networks that incorporates asymmetric mobility between cooperators and defectors through Laplacian-based diffusion (32–34). The model combines localized group interactions, ecological failure of public goods, and network-structured dispersal. Using analytical tools including dispersion relations and amplitude analysis (24, 35, 36), we identify conditions under which homogeneous coexistence becomes unstable and heterogeneous spatial patterns emerge. In this regime, cooperation becomes locally dominant even though the overall system favors defection. Our results further reveal that node connectivity plays a central role in shaping these dynamics, providing a mechanistic explanation for the emergence of cooperative hubs in structured populations. A degree-based mean-field reduction reveals that node connectivity determines an effective coupling strength governing the local dynamics, explaining why highly connected nodes are statistically more likely to sustain cooperative dominance. Together, these findings demonstrate how the interplay between asymmetric mobility and heterogeneous network structure can fundamentally reshape eco-evolutionary dynamics and promote cooperation in complex systems.

1. Mathematical Model

In the framework of ecological public goods (15, 37, 38), we consider a well-mixed population consisting of cooperators and defectors with densities u and v. Interactions occur in randomly formed groups of size N. The multiplication factor of the public good is denoted by $r > 0$, and interactions may fail with probability $z = 1 - u - v$, representing ecological free space. The effective group size is therefore $S = (u + v)N$.

For a defector in a group of size S facing m cooperators, the expected payoff is

$$P_D(S) = \frac{r}{S}\sum_{m=0}^{S-1} m\binom{S-1}{m}\left(\frac{u}{u+v}\right)^m\left(\frac{v}{u+v}\right)^{S-1-m},$$

while the payoff of a cooperator is $P_C(S) = P_D(S) + \frac{r}{S} - 1$.

Averaging over all possible group sizes yields the expected fitness of defectors and cooperators

$$f_D = \frac{ru}{1-z}\left(1 - \frac{1-z^N}{N(1-z)}\right), \qquad f_C = f_D - F(z), \qquad [1]$$

where $F(z) = 1 + (r-1)z^{N-1} - \frac{r}{N}\frac{1-z^N}{1-z}$.

Population densities evolve according to reproductive success. Since reproduction requires available ecological space, it occurs at a rate $z(f_{C,D} + b)$, where b denotes a baseline birth rate that maintains population viability even when payoff contributions are small. Additionally, individuals die at a constant rate d. Combining reproduction and mortality yields the eco-evolutionary dynamics in a single well-mixed population as

$$\begin{aligned}\dot{u} &= u\left(z(f_C + b) - d\right),\\ \dot{v} &= v\left(z(f_D + b) - d\right).\end{aligned} \qquad [2]$$

The detailed construction of the model Eq. **2** is described in *SI Appendix*, section 1. In order to incorporate spatial structure, we embed the system in a complex network of M nodes, each representing a local eco-evolutionary population described by Eq. **2**. Individuals can move between connected nodes, forming a metapopulation framework (39). Let A_{ij} denote the adjacency matrix of the network and $k_i = \sum_j A_{ij}$ the degree of node i. We consider a simple and undirected network, namely among any couple of nodes there can be one or no links at all, moreover the links are reciprocal, hence $A_{ij} = 1$ if and only if there is an undirected link connecting node i and node j, otherwise we set $A_{ij} = 0$. Diffusion between nodes follows Fick's law and depends on density differences across network edges. For a generic variable x_i, the diffusive flux can be written as $\sum_j A_{ij}(x_j - x_i)$, which is equivalent to Laplacian coupling $\sum_j L_{ij}x_j$, where $L_{ij} = A_{ij} - \delta_{ij}k_i$ is the network Laplacian. A system that evolves solely according to this diffusion rule (i.e., $\dot{x}_i = \sum_j L_{ij}x_j$) tries to locally equalize densities in connected nodes (40).

Including this diffusion term yields the networked eco-evolutionary dynamics

$$\begin{aligned}\dot{u}_i &= u_i\left(z_i(f_C + b) - d\right) + \epsilon\sum_{j=1}^{M} L_{ij}u_j,\\ \dot{v}_i &= v_i\left(z_i(f_D + b) - d\right) + \kappa\epsilon\sum_{j=1}^{M} L_{ij}v_j.\end{aligned} \qquad [3]$$

Here u_i and v_i denote the densities of cooperators and defectors at node i, with $z_i = 1 - u_i - v_i$. The parameters ϵ and $\kappa\epsilon$ represent the diffusion rates of cooperators and defectors, respectively, while κ denotes the ratio between the diffusion mobility of defectors and cooperators. This formulation captures the interplay between eco-evolutionary dynamics and diffusion on complex networks.

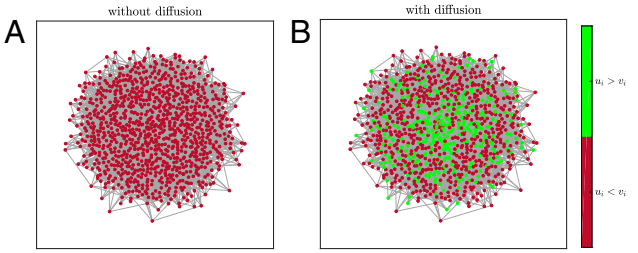

Fig. 1. Impact of asymmetric agents' mobility: We report the result of a simulation of the ecological public goods game where agents interact and diffuse in a scale-free network (BA) of 1,000 nodes and average degree $< k >= 10$. (*A*) shows the emerging network structure when the players cannot diffuse, i.e., $\epsilon = 0$ in Eq. **3**. One can observe that every node becomes a defector-dominated zone, $u_i < v_i$ (deep brown nodes). On the other hand, by inducing the diffusion ability, i.e., $\epsilon > 0$ and $\kappa > 0$, we can appreciate (*B*) the existence of zones where cooperators can outweigh defectors, $u_i > v_i$ (green nodes); let us observe that those nodes have a relatively large degree, while defectors concentrate themselves, $v_i > u_i$, in peripheral nodes, i.e., with smaller degree.

In the subsequent sections, we systematically analyze the emergence of Turing instability (24, 31) in the network-structured eco-evolutionary system described by Eq. **3**. The latter is a general mechanism capable of explaining the emergence of heterogeneous solutions from an initially homogeneous state through diffusion-driven destabilization. In the present work, we investigate this mechanism by performing a linear stability analysis around the stable fixed point of the isolated system Eq. **2**, and then explore the conditions under which diffusion-driven instabilities arise depending on the network topology and diffusion parameters used in Eq. **3**. This instability disrupts the homogeneous coexistence of cooperators and defectors, leading to the spontaneous emergence of spatially heterogeneous patterns across the network nodes. This mechanism provides a deeper understanding of how spatial structure drives pattern formation and evolutionary transitions in eco-evolutionary dynamics.

By anticipating the following analysis, we report in Fig. 1 the outcome of a representative simulation where cooperators and defectors play the ecological public goods game in each node of a scale-free network built using the Barabási-Albert algorithm (BA) (41). In the absence of diffusion (Fig. 1*A*), the dynamics in each node is ruled by Eq. **2**, and the local densities converge to the coexistence equilibrium $u_i = u^*$ and $v_i = v^*$ for all nodes, with $u^* < v^*$. Thus, every node remains defector-prone (brown nodes, represented by $u_i < v_i$), reflecting the defector-dominated coexistence regime. Once diffusion is introduced (Fig. 1*B*), the homogeneous coexistence state becomes unstable and spatial heterogeneity emerges. In particular, a large number of high-degree nodes accumulate a larger fraction of cooperators (green), thereby reversing the local balance to $u_i > v_i$ in those nodes. This diffusion-induced stratification is further investigated in the subsequent section through numerical results and a mean-field analysis. Although defectors dominate globally, mobility asymmetry is associated with enhanced local cooperation in highly connected nodes, increasing local abundance and promoting the spread of cooperation across the network. A comprehensive overview of the temporal effect of agent mobility across the chosen network topology over time is provided in *SI Appendix*, section 7 and Movie S1.

2. Results

This section analyzes the main result shown in Fig. 1 and investigates the impact of the model parameters, r, κ, and N, as well as the network topology, on the system dynamics. Throughout this work, we focus on parameter regimes where the isolated system exhibits a defector-dominated coexistence stable and stationary equilibrium ($u^* < v^*$), allowing us to investigate whether asymmetric mobility and network heterogeneity can enhance cooperation beyond the baseline state.

2.1. Breaking the Stable Coexistence of Competitive Individuals. The eco-evolutionary public-goods framework without mobility, Eq. **2**, exhibits a stationary coexistence of cooperators and defectors at $(u^*, v^*) = (0.020078, 0.102254)$ for the parameter set $r = 4$, $N = 30$, $d = 1.3$, and $b = 1$ (see *SI Appendix*, section 2 and Figs. S1 and S2 for the stability analysis of the aspatial system). In this regime, defectors dominate, consistent with the classical outcome of public-goods games, with v^* nearly five times larger than u^* (horizontal reference lines in Fig. 2*A*). The parameter values considered here are chosen intentionally so that the baseline system remains defector-dominated while still allowing Turing instability and diffusion-driven pattern formation.

A qualitatively different behavior emerges once mobility is introduced, with cooperators and defectors diffusing at different rates. The system is embedded in a scale-free network generated using the Barabási–Albert algorithm with $M = 1{,}000$ nodes and average degree $\langle k \rangle = 10$ (20, 41), where each node hosts the local eco-evolutionary dynamics described by Eq. **2**. For diffusion parameters $\epsilon = 0.01$ and mobility ratio $\kappa = 100$, small heterogeneous perturbations applied to the homogeneous equilibrium of Eq. **3** evolve toward a spatially heterogeneous configuration, breaking the uniform coexistence of cooperators and defectors.

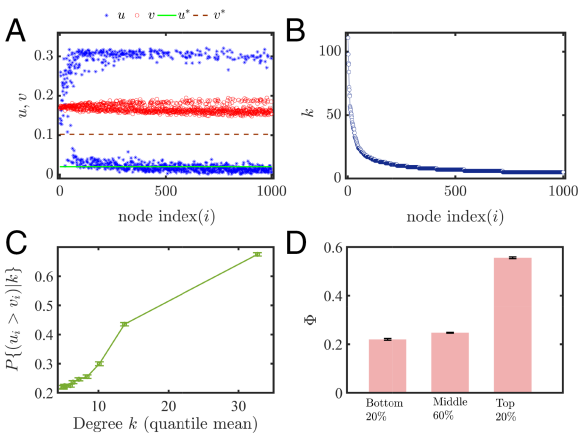

Fig. 2. Diffusion-induced heterogeneous cooperation patterns in a scale-free network. (*A*) Stationary densities of cooperators u_i (blue) and defectors v_i (red) across nodes ordered by decreasing degree. Horizontal lines denote the homogeneous equilibrium values (u^*, v^*) of the aspatial system. Diffusion with asymmetric mobility ($\epsilon = 0.01, \kappa = 100$) produces strong spatial heterogeneity, with several nodes exhibiting cooperative dominance ($u_i > v_i$). (*B*) Degree distribution of the Barabási–Albert network with $M = 1{,}000$ nodes and average degree $\langle k \rangle = 10$, showing the characteristic heavy-tailed connectivity of the scale-free topology. (*C*) $P\{(u_i > v_i)|k\}$, Probability of cooperator-dominated nodes ($u_i > v_i$) as a function of node degree. Nodes are grouped using quantile-based binning, and the horizontal axis represents the mean degree within each bin. Points denote averages over 100 realizations of network structure and initial conditions; error bars indicate the SE. (*D*) Degree-stratified fraction (Φ) of cooperator-dominated nodes in the *Bottom* 20%, *Middle* 60%, and *Top* 20% of the degree distribution. Values represent averages over 100 realizations, with SE bars. Highly connected nodes exhibit a substantially larger probability of cooperative dominance than peripheral nodes.

The temporal development of this instability is illustrated in Movie S1. Initially, node densities remain close to (u^*, v^*), and spatial differentiation is minimal. As time progresses, diffusion amplifies small perturbations about the homogeneous state. Nodes with higher connectivity gradually exhibit increasing cooperative densities, deviating from u^*. The system eventually relaxes to a stationary heterogeneous configuration around $t = 1{,}000$, shown in Fig. 2*A*, where nodes are ordered by decreasing degree. The diffusion-driven instability produces pronounced heterogeneity: Approximately 35% of nodes become cooperator-dominated ($u_i > v_i$), despite the isolated systems favoring defectors. The average asymptotic densities increase to $\langle v \rangle = 0.167271$ and $\langle u \rangle = 0.102184$, compared with the aspatial equilibrium values $v^* = 0.102254$ and $u^* = 0.020078$. Notably, the increase in cooperators is substantially larger than that of defectors, $(\langle u \rangle - u^*) \gg (\langle v \rangle - v^*)$, indicating that asymmetric mobility strongly amplifies cooperative abundance.

The emergence of these heterogeneous patterns is closely related to the network structural heterogeneity. The degree distribution in Fig. 2*B* reflects the heavy-tailed connectivity of the scale-free topology. Visual inspection of Fig. 2*A* suggests that nodes with larger degrees are more likely to exhibit cooperative dominance. This relationship is quantified by measuring the fraction of nodes satisfying $(u_i > v_i)$ as a function of degree (Fig. 2 *C* and *D*). In Fig. 2*C*, nodes are grouped using quantile-based binning of the degree distribution, and the horizontal axis represents the mean degree within each bin. The plotted values, therefore, correspond to the probability that a node is cooperator-dominated within each degree class. Error bars denote the SE computed across multiple realizations of both network structure and initial conditions. Because the degree axis represents quantile averages rather than individual node degrees, the largest value corresponds to the mean degree of the highest quantile group rather than the maximum degree present in the network.

Fig. 2*D* provides a complementary comparison by grouping nodes into three percentile classes: the *Bottom* 20%, the *Middle* 60%, and the *Top* 20% of the degree distribution. The fractions (Φ) of cooperative dominance are again averaged over multiple realizations with SE bars. Both panels show that the probability of cooperative dominance increases with node degree; highly connected nodes (in the top 20%) exhibit more than twice the fraction of cooperative dominance observed among peripheral nodes.

The dependence of cooperation on connectivity is further quantified by evaluating the Pearson correlation between node degree and the binary cooperation indicator $C_i = \mathbf{1}(u_i > v_i)$. Averaged over multiple realizations, a positive correlation ($\rho \approx 0.17$, $P < 10^{-5}$) is obtained, confirming that nodes with higher connectivity are statistically more likely to sustain cooperative dominance. Logistic regression yields the same conclusion: The probability of cooperative dominance increases significantly with node degree. Importantly, this relationship is probabilistic rather than deterministic: While some hubs remain defector-dominated, the likelihood of cooperative dominance increases systematically with node connectivity.

These results indicate that network connectivity plays a key role in shaping the eco-evolutionary dynamics. Nodes with higher degrees experience stronger diffusive coupling with the rest of the network and interact with more neighboring populations. Under asymmetric mobility, this enhanced coupling promotes the local accumulation of slowly diffusing cooperators by increasing the probability that highly connected nodes become cooperator-dominated. This mechanism is consistent with the degree-based mean-field analysis presented later, which shows that increasing node degree increases the effective coupling strength in the reduced dynamics and thereby shifts the local stationary state toward larger cooperator density.

The robustness of the Turing mechanism is tested by repeating the numerical experiments on networks with different topologies, including small-world (Watts–Strogatz) and random (Erdős-Rényi) graphs. The corresponding results (*SI Appendix*, section 3, Figs. S3 and S4, and Movies S2 and S3) show that diffusion destabilizes homogeneous coexistence and produces heterogeneous spatiotemporal patterns across these structures. Although these networks do not exhibit the strong degree of heterogeneity characteristic of scale-free networks, finite realizations still display moderate variability in node connectivity. Consistent with the behavior observed in the scale-free case, nodes with comparatively larger degrees in these networks are also more likely to exhibit cooperative dominance, indicating that the degree-dependent mechanism promoting cooperation is not restricted to scale-free topologies.

Overall, these results demonstrate that asymmetric mobility and heterogeneous network connectivity jointly reshape the eco-evolutionary dynamics of the public-goods game. Diffusion destabilizes the homogeneous equilibrium and promotes the emergence of cooperative clusters, which are preferentially associated with highly connected nodes, providing a structural pathway for cooperation to persist in competitive environments. We note that the parameter regimes considered here yield stationary heterogeneous patterns. Different parameter choices may also produce oscillatory or chaotic diffusion-driven states, as reported in earlier work (15), and remain interesting directions for future investigation.

2.2. Hysteresis and Multistability in Mobility-Induced Pattern Formation. To understand how diffusion asymmetry between cooperators and defectors drives spatial pattern formation in the proposed eco-evolutionary public goods system, we conduct an amplitude analysis by gradually increasing and decreasing the diffusion ratio κ, keeping all the other parameters of individual nodes and network structure the same as in Fig. 2. For each value of κ, we compute the network-wide amplitude A, which measures how far the current state deviates from spatial homogeneity:

$$A = \left[\sum_{i=1}^{M} \left((u_i - u^*)^2 + (v_i - v^*)^2 \right) \right]^{1/2},$$

where u^* and v^* are the steady state densities of the cooperators and defectors, respectively, without diffusion. Let us note that we did not normalize the amplitude with respect to the network size, as we deal with fixed sizes in this work. The amplitude A acts as an indicator of spatial pattern formation: Values close to zero indicate uniform coexistence, while higher values reflect increasing heterogeneity, i.e., the emergence of localized cooperation or defection subgroups.

Fig. 3 displays the results of the amplitude analysis. During forward continuation (blue circles), κ is increased gradually, and the system is allowed to relax to stationarity after each increment. The amplitude remains close to zero until a sharp transition near $\kappa_c \approx 17.55$ emerges, beyond which A rises abruptly, signaling the onset of diffusion-driven spatial pattern formation. Further increases in κ strengthen the heterogeneity (see *Inset R*).

A different behavior appears during backward continuation (red circles), where κ is decreased after reaching the patterned

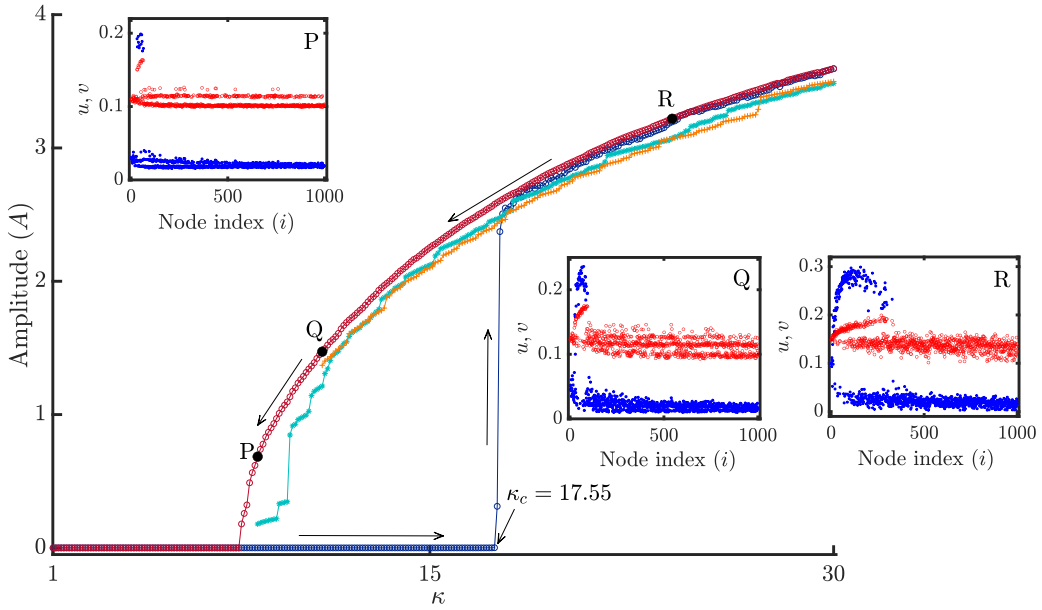

Fig. 3. Amplitude bifurcation reveals hysteresis and multistability in mobility-induced pattern formation. This figure shows the results of an amplitude bifurcation analysis performed on the networked eco-evolutionary public goods system Eq. **3** implemented on a scale-free (BA) network with $M = 1{,}000$ nodes and mean degree $\langle k \rangle = 10$. The system evolved to a stationary equilibrium already at $t = 1{,}000$ time steps for each value of κ, representing the relative mobility of defectors (v) to cooperators (u), while other parameters were held constant at values that maintained stable coexistence in the isolated system. The main panels show the network-averaged amplitude A, which measures the deviation from spatial homogeneity, as a function of κ. Blue hollow circles represent adiabatic forward continuation (increasing κ), where at each step the system is allowed to evolve from a stable fixed point with small perturbations, capturing the emergence of instability. Red hollow circles denote adiabatic backward continuation (decreasing κ), starting from a patterned state and tracking the persistence of spatial structure. A critical threshold $\kappa_c \approx 17.55$ marks the onset of pattern formation through a sharp increase in A. The system exhibits hysteresis: Decreasing κ fails to immediately suppress the pattern, indicating bistability and the presence of multiple attractors—a hallmark of subcritical bifurcation. The figure also includes thin cyan and orange-starred curves that illustrate auxiliary forward and backward continuations under small perturbations, demonstrating sensitivity to initial conditions and network realizations. *Insets* P, Q, and R show the stationary node-wise abundances of cooperators (u, blue) and defectors (v, red) at $\kappa = 8.6$, 11, and 24, respectively. Even at subcritical values below κ_c, strong spatial heterogeneity persists, illustrating the importance of network structure and history dependence.

regime. The system does not immediately return to the homogeneous state but instead remains trapped in patterned configurations even for κ well below the forward threshold (*Insets* P and Q). This mismatch between forward and backward trajectories forms a hysteresis loop, indicating a subcritical bifurcation and multistability between homogeneous and patterned states.

Additional branches (cyan and orange starred curves) are obtained by initializing the system with patterned states P and Q, and performing forward and backward continuations. In these cases, the amplitude increases before the critical value of the main branch, highlighting the sensitivity of pattern emergence to initial conditions and network realization. Similar multibranch structures have been reported in networked Turing systems such as the Mimura–Murray model (24).

The *Insets* of Fig. 3 display representative stationary patterns. Even for $\kappa = 8.6$ and $\kappa = 11$ (corresponding to points P and Q), which lie below the forward critical threshold, strong spatial fluctuations persist, confirming the bistable coexistence of uniform and patterned solutions. Panel R, corresponding to $\kappa = 24$, reveals a well-developed spatial pattern: Groups of high cooperator density emerge in specific zones of the network, particularly among high-degree nodes that are less vulnerable to invasion by fast-moving defectors.

Thus, the bifurcation structure reveals how mobility asymmetry can promote cooperation through spatial differentiation. Rapidly diffusing defectors homogenize the network and deplete shared resources, while slowly diffusing cooperators remain localized, forming protected cooperative clusters. Such mechanisms resemble observations in microbial systems where restricted mobility—e.g., in biofilms or viscous environments—allows cooperative strains producing public goods to persist locally despite global exploitation (10). Similar spatial constraints also promote cooperation in many social and ecological systems.

2.3. The Critical Diffusion Ratio κ_c. The onset of diffusion-driven instability in the eco-evolutionary networked system Eq. **3** is determined by the critical diffusion ratio κ_c. The analytical derivation of this threshold, obtained through the linear stability analysis of the homogeneous coexistence equilibrium (u^*, v^*) and the spectral decomposition of the network Laplacian, is presented in *Materials and Methods*. Here, we summarize the resulting instability condition and its dynamical consequences.

The analysis yields an explicit expression for the critical diffusion ratio,

$$\kappa_c = \frac{f_u g_v - 2 f_v g_u + 2\sqrt{f_v g_u \left(f_v g_u - f_u g_v\right)}}{f_u^2}, \qquad [4]$$

where f_u, f_v, g_u, and g_v denote the elements of the Jacobian matrix of the local eco-evolutionary dynamics evaluated at the homogeneous coexistence equilibrium (u^*, v^*) (Eq. **6**).

The analytical prediction is illustrated in Fig. 4*A*, which shows the maximum $\Lambda^{\max}$ of the dispersion relation as a function of the mobility ratio κ. For small values of κ, $\Lambda^{\max}$ remains negative, indicating that all perturbations decay and the homogeneous coexistence state (u^*, v^*) is linearly stable. As κ increases, $\Lambda^{\max}$ progressively approaches the stability boundary and eventually crosses zero at $\kappa_c \approx 17.55$ (see the black dot in Fig. 4*A*). This crossing point marks the critical threshold beyond which the homogeneous equilibrium loses stability and diffusion-driven spatial heterogeneity can emerge.

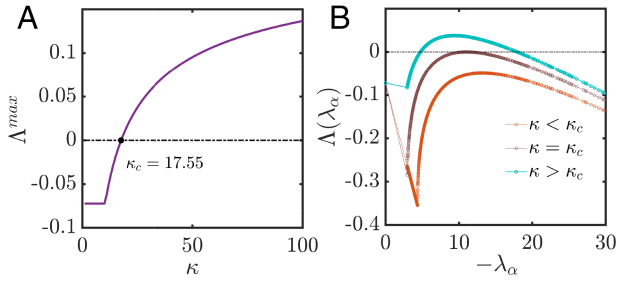

Fig. 4. Analytical characterization of the critical diffusion ratio κ_c: (*A*) Maximum growth rate $\Lambda^{\max}$ as a function of the mobility ratio κ. The curve crosses zero at $\kappa_c \approx 17.55$, which marks the threshold of diffusion-induced instability (marked solid black circle). For $\kappa < \kappa_c$, all perturbations decay and the homogeneous coexistence state remains stable, while beyond this point, instabilities emerge. (*B*) Dispersion relation $\Lambda(\lambda_\alpha)$ for three representative values of κ: Below the threshold ($\kappa < \kappa_c$, orange), exactly at the threshold ($\kappa = \kappa_c$, brown), and above the threshold ($\kappa > \kappa_c$, cyan). Below κ_c, all transverse modes are stable; at $\kappa = \kappa_c$ the leading mode becomes marginally stable; and for $\kappa > \kappa_c$ several modes cross into the positive regime, indicating exponential amplification of spatial perturbations. Together, these panels confirm analytically the onset of Turing instability driven by the mobility of strategy-driven individuals.

Additional insight is provided by Fig. 4*B*, which displays the dispersion relation $\Lambda(\lambda_\alpha)$ (Eq. 7) as a function of $-\lambda_\alpha$, the eigenvalues of the Laplace matrix, for three representative values of the diffusion ratio. When $\kappa < \kappa_c$ (the sea blue curve in Fig. 4*B*), the entire curve lies below zero, implying that all perturbation modes associated with the Laplacian eigenvalues decay and the homogeneous solution remains stable. At $\kappa = \kappa_c$ (see brown curve in Fig. 4*B*), the leading mode horizontally touches the zero line, indicating marginal stability of the system. For $\kappa > \kappa_c$ (orange curve in Fig. 4*B*), part of the dispersion relation becomes positive, meaning that a subset of Laplacian eigenmodes induce exponential growth of any small perturbation and destabilizes the uniform coexistence state.

Taken together, Fig. 4 *A* and *B* confirm that the transition at κ_c corresponds to a genuine diffusion-driven instability. Once the mobility asymmetry between cooperators and defectors exceeds this threshold, the homogeneous eco-evolutionary equilibrium becomes unstable, and spatially heterogeneous patterns can develop across the network.

2.4. Mean-Field Approximation. To explain the numerical patterns observed at large mobility asymmetry and to unravel the degree-dependent organization reported in Fig. 2, we employ a degree-based mean-field approximation similar to those used for reaction–diffusion dynamics on complex networks (24). In this framework, the detailed interactions between a node and its neighbors are replaced by coupling to global mean fields representing the collective state of the network (40, 42–44). The derivation of this method and the computation of the mean fields are provided in *Materials and Methods*.

Under this approximation, the network dynamics reduces to the degree-dependent system

$$\begin{aligned} \dot{u} &= u[(1-u-v)(f_C+b)-d] + \beta(\langle u\rangle - u), \\ \dot{v} &= v[(1-u-v)(f_D+b)-d] + \kappa\beta(\langle v\rangle - v), \end{aligned} \qquad [5]$$

where $\langle u\rangle$ and $\langle v\rangle$ denote the global mean densities of cooperators and defectors, and the effective coupling parameter $\beta = \epsilon k$ is proportional to the node degree k.

The bifurcation structure of this reduced system is shown in Fig. 5*B*. Magenta (cyan) curves denote stable (unstable) stationary branches of the cooperator density, while dark (light) green curves represent stable (unstable) branches of the defector density. As the effective coupling parameter β increases, the system undergoes a saddle-node bifurcation, giving rise to two coexisting stable states over an intermediate range of β. For small values of β, corresponding to weak diffusive coupling, the system remains close to the lower branch associated with the defector-dominated coexistence equilibrium. As β increases beyond the saddle-node threshold, a second stable branch emerges that is characterized by substantially higher cooperator densities.

Because the effective coupling parameter scales linearly with node degree, this bifurcation structure translates directly into degree-dependent dynamics on the network. Fig. 5*A* compares the stationary cooperator densities obtained from full network simulations (red crosses) with the stationary branches predicted by the mean-field equations (magenta curves) evaluated at $\beta_i = \epsilon k_i$ for $\epsilon = 0.01$ and $\kappa = 100$. In the mean-field description, each node i is therefore characterized by its own bifurcation parameter value determined by its degree. The stationary network pattern can thus be interpreted as a set of points distributed along the bifurcation diagram of the reduced system.

The comparison reveals a clear separation between low- and high-degree nodes. Nodes with small degree cluster near the lower stable branch corresponding to defector-dominated coexistence, whereas highly connected nodes populate the upper stable branch associated with enhanced cooperator density. Although some scattering of numerical data appears near the bifurcation points, the overall agreement between simulation results and mean-field predictions demonstrates that the heterogeneous network pattern is well explained by the bifurcation structure of a single node coupled to the global mean fields, with the effective coupling strength determined by the node degree.

Remarkably, the bifurcation structure also shows multistability. Over an intermediate range of the coupling parameter β, both stationary branches coexist as stable solutions. Consequently, nodes with similar degrees may converge to different stationary states depending on perturbations or initial conditions. This explains why, although the probability of cooperative dominance increases with node degree (Fig. 2), not all hubs become cooperator-dominated in the network simulations.

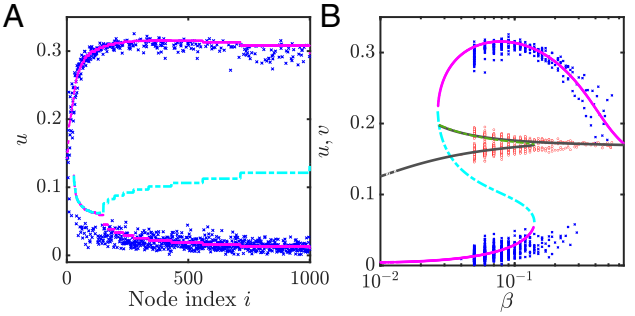

Fig. 5. Degree-based mean-field approximation and bifurcation structure: (*A*) shows the degree-resolved stationary cooperator densities u_i plotted against the ordered node index (ordered by decreasing degree) for $\kappa = 100$ and $\epsilon = 0.01$. Blue crosses denote the cooperator densities from full network simulations, while the magenta (cyan) curves represent the corresponding stationary stable (unstable) solutions obtained from the reduced mean-field equation. (*B*) shows the bifurcation diagram of the reduced mean-field system as a function of the effective coupling parameter $\beta = \epsilon k$ for $\epsilon = 0.01$. Magenta (cyan) curves denote stable (unstable) stationary branches of cooperators, while dark (light) green curves represent stable (unstable) branches of defectors. Blue crosses and red circles depict the cooperator and defector densities from network simulation for $\kappa = 100$ and $\epsilon = 0.01$. A saddle-node bifurcation generates two coexisting stable states over an intermediate range of β, explaining the emergence of cooperative dominance over high-degree nodes and the multistable behavior observed in the network simulations.

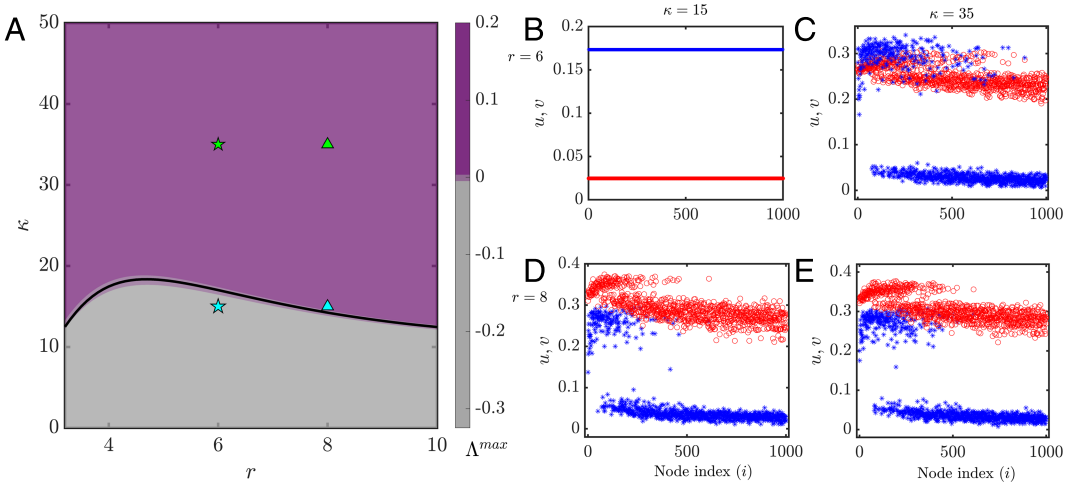

Fig. 6. Diffusion-induced instability in (r, κ) parameter space. We show the maximum of the dispersion relation $\Lambda^{\max}$ as a function of r and κ, as computed from the theory presented in Section 2.3. The latter indicates regions of stability and instability in the eco-evolutionary public goods system. In (*A*) purple region correspond to unstable regimes where $\Lambda^{\max}(\kappa, r) > 0$ and spatial patterns emerge; gray regions indicate stable coexistence ($\Lambda^{\max}(\kappa, r) < 0$). The analysis is performed for $\epsilon = 0.01$, $N = 30$, $b = 1$, $d = 1.3$ on a scale-free network ($N = 1{,}000$, $\langle k \rangle = 10$). Patterns are most likely to emerge in intermediate ranges of the public goods multiplication factor r and diffusion ratio κ. The black curve represents the critical curve of κ_c, obtained from Eq. **4**. The numerical validations for various combinations of (r, κ), distinguished by different colors and markers, are shown in (*B–E*). Here, cyan, and light green markers represent $\kappa = 15$, and 35, respectively, whereas stars, and triangles correspond to $r = 6$, and 8, respectively. Each panel shows u (blue) and v (red) for all 1,000 nodes. At low κ (*B*), the system remains homogeneous; as κ increases (*C*), spatial heterogeneity emerges with pronounced local fluctuations. Notably, higher r values correlate with reduced cooperation levels (*D* and *E*), especially at high κ, highlighting how group-size dilution undermines cooperation in real-world public goods dilemmas.

3. Impact of the Multiplication Factor r and Diffusion Ratio κ on Diffusion-Driven Instability

To further understand how cooperative amplification and mobility asymmetry jointly shape the emergence of spatial patterns, we analyze the stability of the homogeneous state by calculating the maximum of the dispersion relation $\Lambda^{\max}$ in the two-dimensional parameter space defined by the public goods multiplication factor r and the diffusion ratio κ. The sign of $\Lambda^{\max}$ determines the stability of the homogeneous equilibrium of system Eq. **3**: Negative values correspond to stable homogeneous dynamics, whereas $\Lambda^{\max} > 0$ signals diffusion-driven instability.

The analytical stability diagram is shown in Fig. 6*A*. The black solid curve represents the critical diffusion ratio $\kappa_c(r)$ obtained from Eq. **4**. This curve separates the stable regime, $\Lambda^{\max} < 0$, from the instability region, $\Lambda^{\max} > 0$, where diffusion destabilizes the homogeneous coexistence equilibrium and spatial heterogeneity may develop. The dependence of κ_c on r is nonmonotonic: The threshold initially increases with r, reaches a maximum near $r \approx 5$, and then decreases. Consequently, sufficiently large diffusion asymmetry destabilizes the homogeneous state over a broad range of multiplication factors.

To illustrate this analytical prediction, four representative parameter combinations were selected and marked in Fig. 6*A*. Two values of the multiplication factor were considered, $r = 6$ and $r = 8$, together with two diffusion ratios, $\kappa = 15$ and $\kappa = 35$. The points $(6, 15)$ and $(8, 15)$ are indicated by cyan symbols (star and triangle), while $(6, 35)$ and $(8, 35)$ are represented by light-green symbols (star and triangle). The corresponding numerical simulations are shown in Fig. 6 *B–E*, where the stationary densities of cooperators (u_i) and defectors (v_i) are plotted across the $M = 1{,}000$ nodes of the network. For the parameter set $(6, 15)$, located below the instability boundary, the system converges to a homogeneous state, as shown in Fig. 6*B*. In contrast, the remaining three parameter combinations lie above the analytical threshold $\kappa_c(r)$ and produce spatially heterogeneous states, visible in Fig. 6 *C–E*.

These results confirm that the instability condition $\kappa > \kappa_c(r)$ predicted by the analytical dispersion relation accurately determines the emergence of heterogeneous cooperative patterns. The agreement between the analytical stability boundary and the numerical outcomes demonstrates that asymmetric mobility between cooperators and defectors destabilizes the homogeneous eco-evolutionary equilibrium and generates spatial organization across the network.

The results also reveal that increasing the multiplication factor r does not always promote cooperation once spatial dynamics are present (Fig. 6 *D* and *E*). In some regimes, larger r reduces cooperative density because amplified group benefits increase defectors' exploitation. Thus, cooperation persists not simply through higher rewards but through spatial segregation enabled by mobility asymmetry. Taken together, the analytical stability map and numerical simulations show that cooperation emerges within a structured region of the (r, κ) parameter space, where payoff amplification and differential mobility destabilize the homogeneous state and allow cooperative clusters to persist.

4. Conclusions and Discussions

In this study, we introduced and analyzed an eco-evolutionary public goods game model on complex networks, focusing on the role of asymmetric diffusion between cooperators and defectors. By combining localized group interactions, ecological constraints, and network-structured mobility, the model provides a comprehensive framework to investigate how cooperation can emerge and persist in spatially structured populations.

A central outcome of our investigation is that the faster diffusion of defectors relative to cooperators destabilizes homogeneous coexistence in which defectors dominate, leading to a symmetry-breaking transition and the emergence of a self-organized, cooperation-rich population. These patterns were validated numerically through amplitude bifurcation analysis and analytically supported by the dispersion relation, which together illustrate how heterogeneous network topology underlies the formation of spatially localized cooperative zones: Highly connected

nodes exhibit a higher probability of cooperative dominance, while peripheral nodes remain more susceptible to defector invasion.

To explain this mechanism, we developed a degree-based mean-field description of the network dynamics. The analysis shows that the effective coupling strength experienced by each node scales with its degree. Consequently, nodes with different degrees effectively operate at different positions along the bifurcation diagram of the reduced system. The bifurcation analysis reveals a saddle-node structure that produces bistability between a defector-dominated state and a cooperative state. This theoretical prediction accurately reproduces the heterogeneous patterns observed in the full network simulations and explains why cooperation tends to emerge preferentially in highly connected nodes. At the same time, the presence of multistability implies that transitions are probabilistic rather than deterministic, so that not all hubs necessarily become cooperator-dominated.

Importantly, the system also exhibits hysteresis. Once spatial cooperation patterns are established, reversing the conditions that initially led to their formation does not necessarily return the system to its original state. This path dependence highlights the strong influence of initial conditions and perturbations on shaping long-term dynamics, revealing a landscape of alternative stable states. The agreement between numerical simulations and analytical predictions further reinforces the generality of these behaviors. It is important to note that the present study focuses on representative parameter regimes that allow diffusion-driven instability in the baseline defector-dominated system. Although the analytical treatment captures the onset of instability and the degree-dependent organization of the stationary patterns, it does not provide a complete analytical characterization of the full parameter space nor a derivation of the increase in global average densities. Extending the theory in these directions remains an important topic for future work.

A comprehensive exploration of the parameter space, including the synergy factor (r), group size (N), and diffusion asymmetry ratio (κ), reveals that cooperation is maximized through a nuanced balance among these factors. While a higher r tends to promote cooperation, it can also increase susceptibility to defection without spatial support. Larger group sizes amplify collective benefit but may dilute individual payoffs (*SI Appendix*, section 4 and Fig. S5), and diffusion asymmetry broadens the range of instability, enabling richer pattern dynamics. Together, these parameters define a complex regime in which cooperation emerges through spatial differentiation rather than mean-field expectations.

From an eco-evolutionary perspective, our findings demonstrate that the interplay between asymmetric mobility and heterogeneous connectivity provides a powerful mechanism for promoting cooperation in structured populations. Such mechanisms are relevant for a variety of ecological and social systems, including microbial communities, collective resource management, and social interaction networks, where mobility and structural heterogeneity influence cooperative behavior.

In conclusion, our study underscores the need to incorporate spatial heterogeneity, mobility asymmetry, and network topology into models of eco-evolutionary dynamics. By combining large-scale simulations with analytical techniques, we show how structured populations can defy classical expectations, allowing cooperation to thrive even under ecologically adverse conditions. These findings offer practical insights into designing strategies for fostering cooperation in real-world systems, ranging from microbial ecosystems to social networks, by leveraging control over mobility, interaction structure, and group composition. Looking ahead, the generality of our framework invites verification across additional network classes and empirical interaction topologies, thus representing a promising avenue for future research, with the potential to further deepen our understanding of how cooperation emerges and persists under diverse ecological and social conditions. Let us conclude by emphasizing another possible direction, rooted in a more realistic diffusion process; indeed Eq. **3** models a linear diffusion process, while rational agents would decide where to go or which nodes to avoid, for instance, cooperators could be less prone to move toward nodes with a larger density of defectors. This behavior can be included by replacing the linear diffusion terms in Eq. **3** with a nonlinear one, e.g., $\dot{u}_i \sim \epsilon \sum_j L_{ij} h(u_j, v_j)$ where h is some nonlinear function encoding the rational choice of the players; a similar term can be inserted for the evolution rate of v_i.

5. Materials and Methods

5.1. Linear Stability Analysis and Critical Diffusion Ratio. To determine the onset of diffusion-driven instability discussed in Section 2.3, we perform a linear stability analysis of the networked eco-evolutionary system Eq. **3** about the homogeneous coexistence equilibrium $x^* = (u^*, v^*)$ of the isolated dynamics Eq. **2**.

We introduce small perturbations at each node, $\delta x_i = (\delta u_i, \delta v_i)^\top$, defined as $\delta u_i = u_i - u^*$, $\delta v_i = v_i - v^*$. Substituting these expressions into Eq. **3** and retaining only first-order terms yields

$$\frac{d}{dt}\delta x_i = J_F(x^*)\,\delta x_i + \sum_{j=1}^{M} L_{ij} D\,\delta x_j,$$

where $J_F(x^*)$ is the Jacobian matrix of the local eco-evolutionary dynamics evaluated at (u^*, v^*), i.e., $J_F(x^*) = \begin{pmatrix} f_u & f_v \\ g_u & g_v \end{pmatrix}$, and $D = \begin{pmatrix} \epsilon & 0 \\ 0 & \kappa\epsilon \end{pmatrix}$ is the diffusion matrix describing the asymmetric mobility of cooperators and defectors.

Because the Laplacian matrix L is diagonalizable, the perturbations can be expanded in its eigenbasis. Let λ_α denote the Laplacian eigenvalues, and δy_α the amplitude of the perturbation along the eigenvector corresponding to mode α. Because the Laplacian matrix L is diagonalizable, the perturbations can be expanded in its eigenbasis. Let λ_α denote the Laplacian eigenvalues, and δy_α the coefficient of the perturbation along the eigenvector $\phi^{(\alpha)}$ associated with λ_α. The perturbation modes then decouple as

$$\frac{d}{dt}\delta y_\alpha = \left[J_F(x^*) + \lambda_\alpha D\right]\delta y_\alpha \equiv J_\alpha \delta y_\alpha. \qquad [6]$$

The stability of each mode is determined by the eigenvalues of the matrix J_α. We therefore define the dispersion relation

$$\Lambda(\lambda_\alpha) = \max \Re\left[\sigma(J_\alpha)\right], \qquad [7]$$

where $\sigma(J_\alpha)$ denotes the spectrum of J_α. The homogeneous equilibrium is stable when $\Lambda(\lambda_\alpha) < 0$ for all transverse modes $\alpha > 1$. Conversely, diffusion-driven instability occurs if $\Lambda(\lambda_\alpha) > 0$ for some mode. In other words, The dispersion relation, $\Lambda(\lambda_\alpha)$ solves

$$\begin{aligned}\Lambda^2 - \Lambda\left[\mathrm{tr}(J_F(x^*)) + \epsilon\lambda_\alpha(1+\kappa)\right] + \det(J_F(x^*)) \\ + \epsilon\lambda_\alpha(g_v + \kappa f_u) + \epsilon^2\lambda_\alpha^2\kappa = 0,\end{aligned} \qquad [8]$$

where to lighten the notation we did not write explicitly the dependence of Λ on λ_α. The critical κ_c is the value of κ at which the dispersion relation has a double zero, namely the curve $\Lambda(\lambda_\alpha)$ touches the horizontal axis at $\lambda_\alpha^{(c)}$ and has a horizontal tangent at this point. Mathematically, this condition can be realized by imposing

$$\Lambda(\lambda_\alpha^{(c)}) = 0 \quad \text{and} \quad \frac{\partial\Lambda}{\partial\lambda_\alpha}\Big|_{\lambda_\alpha^{(c)}} = 0.$$

By using the definition Eq. **8** and by performing the derivative, one can obtain the following two conditions:

$$\begin{aligned} \det(J_F(x^*)) + \epsilon\lambda_\alpha^{(c)}(g_v + \kappa_c f_u) + \epsilon^2(\lambda_\alpha^{(c)})^2\kappa_c &= 0, \\ \epsilon(g_v + \kappa_c f_u) + 2\epsilon^2\lambda_\alpha^{(c)}\kappa_c &= 0, \end{aligned} \quad [9]$$

After some straightforward algebraic manipulations, we get

$$\kappa_c = \frac{f_u g_v - 2f_v g_u + 2\sqrt{f_v g_u(f_v g_u - f_u g_v)}}{f_u^2}. \quad [10]$$

This analytical threshold, determined from Eq. **10**, determines when diffusion destabilizes the homogeneous coexistence state, as illustrated in Fig. 4 and discussed in Section 2.3.

Let us observe that, as a byproduct, we have also been able to compute the critical eigenvalue $\lambda_\alpha^{(c)}$ that realizes the double zero of the dispersion relation. In conclusion, for all $\kappa < \kappa_c$, the dispersion relation is negative and patterns cannot emerge. On the other hand $\kappa > \kappa_c$ is a necessary condition to have patterns; indeed, because of finite size effects, one must ensure the existence of Laplace eigenvalues, λ_α, for which $\Lambda(\lambda_\alpha) > 0$, the latter depends on the size of the network, on its topology but also on the model parameters (*SI Appendix*, section 5 and Fig. S6).

5.2. Degree-Based Mean-Field Approximation. To analyze the heterogeneous spatial patterns observed numerically and analyzed in Section 2.4, we employ a degree-based mean-field approximation applied to the studied networked system Eq. **3**. Using the definition of the Laplacian, the diffusive coupling term can be rewritten as $\sum_j L_{ij}u_j = \sum_j A_{ij}(u_j - u_i)$. Defining the average state of the neighbors of node i as $\bar{u}_i = \frac{1}{k_i}\sum_j A_{ij}u_j$, the diffusion term becomes $\sum_j A_{ij}(u_j - u_i) = k_i(\bar{u}_i - u_i)$. An analogous relation holds for the defector density v_i. Following the mean-field approximation commonly used for reaction–diffusion systems on complex networks (24, 42), the neighbor average is approximated by a global degree-weighted mean field. We define

$$\langle u\rangle = \frac{\sum_j k_j u_j}{\sum_j k_j}, \qquad \langle v\rangle = \frac{\sum_j k_j v_j}{\sum_j k_j}, \quad [11]$$

which represent the degree-weighted average densities of cooperators and defectors. This approximation accounts for the fact that highly connected nodes contribute more to a node's typical neighborhood. Under this assumption, $\bar{u}_i \approx \langle u\rangle$, $\bar{v}_i \approx \langle v\rangle$. Substituting these expressions into the diffusion terms yields the reduced network dynamics as

$$\begin{aligned} \dot{u}_i &= u_i[(1 - u_i - v_i)(f_C + b) - d] + \epsilon k_i(\langle u\rangle - u_i), \\ \dot{v}_i &= v_i[(1 - u_i - v_i)(f_D + b) - d] + \kappa\epsilon k_i(\langle v\rangle - v_i). \end{aligned} \quad [12]$$

Introducing the effective coupling parameter $\beta_i = \epsilon k_i$, the reduced equations can be written as

$$\begin{aligned} \dot{u} &= u[(1 - u - v)(f_C + b) - d] + \beta(\langle u\rangle - u), \\ \dot{v} &= v[(1 - u - v)(f_D + b) - d] + \kappa\beta(\langle v\rangle - v), \end{aligned} \quad [13]$$

where we have omitted the index i, as all nodes follow the same equation. Within this approximation, nodes with different degrees experience different effective coupling strengths $\beta = \epsilon k$. Consequently, the heterogeneous network can be interpreted as an ensemble of identical eco-evolutionary systems evolving at different values of the control parameter β. The stationary states of the reduced system can therefore be analyzed using bifurcation methods, allowing the degree-dependent organization observed in the network simulations to be interpreted in terms of the bifurcation structure shown in Fig. 5.

Here, the global mean fields for cooperators, $\langle u\rangle$, and defectors, $\langle u\rangle$, are obtained self-consistently from the stationary patterned state of the full network dynamics Eq. **3**. The network system is first numerically integrated until a stationary configuration is reached. The global mean densities of cooperators and defectors are then computed as degree-weighted averages across all nodes and substituted into the reduced mean-field equations Eq. **13**. For fixed values of these mean fields, the stationary states of a node with a given degree are obtained from the steady-state conditions of the mean-field system. This yields degree-dependent branches of stationary solutions whose stability depends on the system parameters. The stability of these solutions is determined from the Jacobian matrix of the mean-field system evaluated at the stationary states. The eigenvalues of the Jacobian characterize the stability of the solution branches, while saddle-node bifurcations occur when the determinant of the Jacobian vanishes, marking the appearance or disappearance of stationary states as the node degree varies. The resulting bifurcation structure provides the theoretical curves used to interpret the numerical results in Fig. 5. We emphasize that the mean-field approximation captures the degree-dependent organization of the stationary patterns once the global mean densities are specified. However, the theory does not explain the increase in the average densities beyond the homogeneous equilibrium values, which is observed numerically.

We further note that this mean-field approximation is not restricted to scale-free networks. A similar agreement is observed between the reduced equations and full network simulations for other network topologies, including small-world and random networks; these results are presented in *SI Appendix*, section 6 and Figs. S7–S9. It is also important to note that the mean-field theory is generally not applicable for localized patterns below the instability threshold (24).

Data, Materials, and Software Availability. The codes that were used for the findings of this study are openly available in the GitHub repository (45). All other data are included in the manuscript and/or supporting information.

ACKNOWLEDGMENTS. M.P. was supported by the Slovenian Research and Innovation Agency (Grant No. P1-0403). M.S.A. would like to thank Anusandhan National Research Foundation, Department of Science & Technology, Government of India, for providing financial support in terms of a National Post Doctoral Fellowship (File Number: PDF/2025/003667). M.S.A. would also like to thank the Indian Statistical Institute, Kolkata, and the Indian Institute of Technology Bombay for financial support during the preparation of the manuscript. We thank the reviewers for their insightful comments and constructive suggestions, which have significantly improved the manuscript.

Author affiliations: [a]Bagchi School of Public Health, Ahmedabad University, Ahmedabad, Gujarat 380009, India; [b]Department of Physical Sciences, Indian Institute of Science Education and Research Kolkata, Mohanpur, Nadia, West Bengal 741246, India; [c]Department of Mathematics, Namur Institute for Complex Systems–naXys, University of Namur, Namur B 5000, Belgium; [d]Faculty of Natural Sciences and Mathematics, University of Maribor, Maribor 2000, Slovenia; [e]Community Healthcare Center Dr. Adolf Drolc Maribor, Maribor 2000, Slovenia; [f]Department of Physics, Kyung Hee University, Dongdaemun-gu, Seoul 02447, Republic of Korea; [g]University College, Korea University, Seongbuk-gu, Seoul 02841, Republic of Korea; and [h]Physics and Applied Mathematics Unit, Indian Statistical Institute, Kolkata 700108, India

Author contributions: M.S.A. designed the research; S.R. and M.S.A. performed the research; S.R., M.S.A., and T.C. contributed to the analytical results; S.R., M.S.A., T.C., M.P., and D.G. analyzed data; and S.R., M.S.A., T.C., M.P., and D.G. wrote the paper.

1. A. Szolnoki, M. Perc, Reward and cooperation in the spatial public goods game. *Europhys. Lett.* **92**, 38003 (2010).
2. D. Balduzzi *et al.*, "The mechanics of n-player differentiable games" in *International Conference on Machine Learning*, J. Dy, A. Krause, Eds. (PMLR, 2018), vol. **80**, pp. 354–363.
3. M. A. Nowak, Five rules for the evolution of cooperation. *Science* **314**, 1560–1563 (2006).
4. G. Szabó, C. Hauert, Phase transitions and volunteering in spatial public goods games. *Phys. Rev. Lett.* **89**, 118101 (2002).
5. G. Hardin, "The tragedy of the commons" in *Classic Papers in Natural Resource Economics Revisited*, C. Gopalakrishnan, Ed. (Routledge, 2018), pp. 145–156.
6. E. Ostrom, Tragedy of the commons. *New Palgrave Dict. Econ.* **2**, 1–4 (2008).
7. S. Sohel Mondal, A. Ray, S. Chakraborty, Hypochaos prevents tragedy of the commons in discrete-time eco-evolutionary game dynamics. *Chaos Interdiscip. J. Nonlinear Sci.* **34**, 023122 (2024).
8. M. A. Nowak, "Evolutionary dynamics of cooperation" in *Proceedings of the International Congress of Mathematicians* (European Mathematical Society, Zürich, 2006), vol. 3, pp. 1523–40.
9. C. D. Nadell, K. Drescher, K. R. Foster, Spatial structure, cooperation and competition in biofilms. *Nat. Rev. Microbiol.* **14**, 589–600 (2016).
10. J. Cremer *et al.*, Chemotaxis as a navigation strategy to boost range expansion. *Nature* **575**, 658–663 (2019).

11. D. G. Rand *et al*., Social heuristics shape intuitive cooperation. *Nat. Commun.* **5**, 3677 (2014).
12. S. Roy *et al*., Time delays shape the eco-evolutionary dynamics of cooperation. *Sci. Rep.* **13**, 14331 (2023).
13. K. Betz, F. Fu, N. Masuda, Evolutionary game dynamics with environmental feedback in a network with two communities. *Bull. Math. Biol.* **86**, 84 (2024).
14. S. N. Chowdhury, S. Kundu, J. Banerjee, M. Perc, D. Ghosh, Eco-evolutionary dynamics of cooperation in the presence of policing. *J. Theor. Biol.* **518**, 110606 (2021).
15. J. Y. Wakano, M. A. Nowak, C. Hauert, Spatial dynamics of ecological public goods. *Proc. Natl. Acad. Sci. U.S.A.* **106**, 7910–7914 (2009).
16. J. Y. Wakano, C. Hauert, Pattern formation and chaos in spatial ecological public goodsgames. *J. Theor. Biol.* **268**, 30–38 (2011).
17. D. J. Hernandez, A. S. David, E. S. Menges, C. A. Searcy, M. E. Afkhami, Environmental stress destabilizes microbial networks. *ISME J.* **15**, 1722–1734 (2021).
18. J. Pan, L. Zhang, W. Han, C. Huang, Heterogeneous investment promotes cooperation in spatial public goods game on hypergraphs. *Phys. A Stat. Mech. Appl.* **609**, 128400 (2023).
19. D. L. Pires, M. Broom, The rules of multiplayer cooperation in networks of communities. *PLoS Comput. Biol.* **20**, e1012388 (2024).
20. A. L. Barabási, E. Bonabeau, Scale-free networks. *Sci. Am.* **288**, 60–69 (2003).
21. D. J. Watts, S. H. Strogatz, Collective dynamics of 'small-world' networks. *Nature* **393**, 440–442 (1998).
22. J. Andreas, M. Rohrbach, T. Darrell, D. Klein, "Neural module networks" in *Proceedings of the IEEE Conference on Computer Vision and Pattern Recognition* (IEEE Computer Society, Los Alamitos, CA, 2016), pp. 39–48.
23. F. C. Santos, J. M. Pacheco, Scale-free networks provide a unifying framework for the emergence of cooperation. *Phys. Rev. Lett.* **95**, 098104 (2005).
24. H. Nakao, A. S. Mikhailov, Turing patterns in network-organized activator-inhibitor systems. *Nat. Phys.* **6**, 544–550 (2010).
25. S. Gao, L. Chang, M. Perc, Z. Wang, Turing patterns in simplicial complexes. *Phys. Rev. E* **107**, 014216 (2023).
26. E. A. Stanley, D. Ashlock, M. D. Smucker, "Iterated prisoner's dilemma with choice and refusal of partners: Evolutionary results" in *European Conference on Artificial Life*, F. Morán, A. Moreno, J. J. M. Guervós, P. Chacón, Eds. (Springer, 1995), pp. 490–502.
27. D. Ashlock, M. D. Smucker, E. A. Stanley, L. Tesfatsion, Preferential partner selection in an evolutionary study of prisoner's dilemma. *BioSystems* **37**, 99–125 (1996).
28. M. Hu, W. Chen, Collective-risk social dilemma on the risk-driven dynamic networks. *Chaos Solitons Fractals* **184**, 115058 (2024).
29. G. Zhang, Y. Yao, Z. Zeng, M. Feng, M. Chica, The evolution of cooperation in spatial public goods game with tolerant punishment based on reputation threshold. *Chaos Interdiscip. J. Nonlinear Sci.* **35**, 013104 (2025).
30. H. Cheng *et al*., Evolution of cooperation in spatio-temporal evolutionary games with public goods feedback. *Bull. Math. Biol.* **86**, 67 (2024).
31. A. Turing, The chemical basis of morphogenesis. *Philos. Trans. R. Soc. Lond. B* **237**, 37 (1952).
32. C. S. Gokhale, A. Traulsen, Evolutionary games in the multiverse. *Proc. Natl. Acad. Sci. U.S.A.* **107**, 5500–5504 (2010).
33. C. S. Gokhale, C. Hauert, Eco-evolutionary dynamics of social dilemmas. *Theor. Popul. Biol.* **111**, 28–42 (2016).
34. R. Merris, Laplacian matrices of graphs: A survey. *Linear Algebr. Appl.* **197**, 143–176 (1994).
35. M. Asllani, D. M. Busiello, T. Carletti, D. Fanelli, G. Planchon, Turing patterns in multiplex networks. *Phys. Rev. E* **90**, 042814 (2014).
36. R. Muolo, L. Giambagli, H. Nakao, D. Fanelli, T. Carletti, Turing patterns on discrete topologies: From networks to higher-order structures. *Proc. R. Soc. A.* **480**, 20240235 (2024).
37. C. Hauert, M. Holmes, M. Doebeli, Evolutionary games and population dynamics: Maintenance of cooperation in public goods games. *Proc. R. Soc. B Biol. Sci.* **273**, 2565–2571 (2006).
38. C. Hauert, J. Y. Wakano, M. Doebeli, Ecological public goods games: Cooperation and bifurcation. *Theor. Popul. Biol.* **73**, 257–263 (2008).
39. R. May, Will a large complex system be stable? *Nature* **238**, 413 (1972).
40. A. Barrat, M. Barthelemy, A. Vespignani, *Dynamical Processes on Complex Networks* (Cambridge University Press, 2008).
41. R. Albert, A. L. Barabási, Statistical mechanics of complex networks. *Rev. Mod. Phys.* **74**, 47–97 (2002).
42. H. Nakao, A. S. Mikhailov, Diffusion-induced instability and chaos in random oscillator networks. *Phys. Rev. E* **79**, 036214 (2009).
43. V. Colizza, R. Pastor-Satorras, A. Vespignani, Reaction-diffusion processes and metapopulation models in heterogeneous networks. *Nat. Phys.* **3**, 276–282 (2007).
44. V. Colizza, A. Vespignani, Epidemic modeling in metapopulation systems with heterogeneous coupling pattern: Theory and simulations. *J. Theor. Biol.* **251**, 450–467 (2008).
45. S. Roy, M. S. Anwar, T. Carletti, M. Perc, D. Ghosh, Diffusion-induced instabilities promote cooperation in eco-evolutionary networks. Zenodo. https://doi.org/10.5281/zenodo.20844369. Accessed 21 May 2026.